Estimating the Outflow Discharge Rate from Landslide Dam Outbursts

Takahisa Mizuyama,[1)] Yoshifumi Satohuka,[1)] Kiichiro Ogawa[2)] and Toshio Mori[3)]
1) Graduate School of Agriculture, Kyoto University, Oiwake-cho, Kitashirakawa, Sakyo-ku, Kyoto 606-8502 (mizuyama@kais.kyoto-u.ac.jp)
2) Asia Air Survey Co., LTD, Manpukuji 1-2-2, Azabu, Kawasaki, Kanagawa 215-0004 (ki.ogawa@ajiko.co.jp)
3) Sabo Frontier Foundation, Sabo-kaikan, Hirakawa-cho 2-7-4, Chiyoda-ku, Tokyo 102-0093 (rijicyou@sff.or.jp)

Abstract

Landslides and debris flows generated by heavy rainfalls and earthquakes, sometimes block waterways and form landslide dams. Most landslide dams are filled with water and experience overflow. However, outbursts of these dams may result in large floods or debris flows, endangering residents in downstream, flood-prone areas.

Evacuations of these areas may be recommended when landslide dams form. It is thus necessary to estimate outflow discharge rates as rapidly as possible. Empirical methods based on past events and theoretical methods have been developed to estimate outflow discharge. However, these models are not sufficiently accurate for practical use. Some of the landslide dams formed by the Chuetsu earthquake that struck Niigata Prefecture, Japan, in October 2004 have been observed and surveyed. Erosion processes associated with landslide dam overflow have been investigated using flume experiments. Numerical analyses of slope stability for various landslide dam dimensions and conditions have also been conducted and past landslide dams have been surveyed. Based on the results of these studies, a numerical simulation model was developed to estimate both peak flow and the flow hydrograph. The model also calculated downstream deposition. The method was applied to a historical flood resulting from the outburst of the Taka-iso-yama landslide dam in the Naka River of Shikoku. The calculated results agreed well with field data. This modeling method will be applied to actual risk management activities. Topographic information on new landslide dams obtained using a laser profiling technique will be input to the model calculations.

Keywords: landslide dam, outburst, flood discharge, simulation, flume experiments

Introduction

Landslides and debris-flows can block mountain streams to form landslide dams. While these processes do not always lead to abrupt dam collapse and downstream flooding, they can threaten and concern downstream residents. It is therefore necessary to estimate these processes and to accurately predict peak flood discharge. The 2004 Chuetsu earthquake in Japan caused many landslide dams particularly in the Imo River basin. Peak flow discharge was predicted and people were evacuated. Fortunately major landslide dams did not collapse owing to the low winter rainfall amount and emergency drainage measures. To improve prediction and reaction techniques, flume experiments, slope stability analysis and computer simulation were carried out. This paper presents some of the results.

Experiments on outburst processes and outflow discharge

Landslide dam models were constructed in a flume with a width of 30 cm, side wall gradient of 1:0.7, and flume gradient of 11.3° (Figure 1). The landslide dam models were made of sand or sand with bentonite as cohesive materials. A 2.0-cm wide and 2.0-cm deep trench was prepared in the center of the landslide dam crest.

Conditions are given in Table 1. The grain size distribution of the sand is shown in Figure 2. Bentonite concentrations were fixed at 2.5 %, because higher percentages made the mixture too strong.

Figure 3 shows the outflow discharge resulting from these experiments. The experiment using only sand (no bentonite) had the largest outflow discharge, 17 times greater than the inflow water discharge. The downstream bank gradient had relatively little influence on the outflow discharge. Landslides did not occur when water flowed over landslide dams. Landslide dams were usually much longer longitudinally than artificial

pp. 365–377

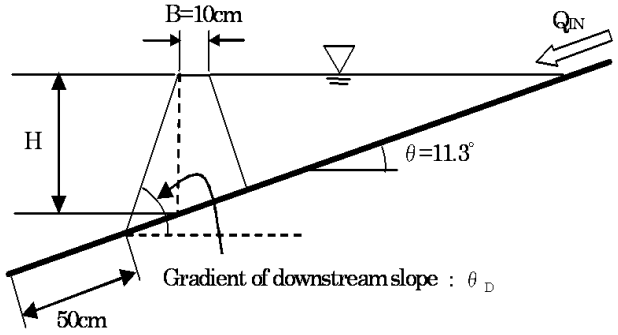

Fig. 1. Installing a landslide dam in a trapezoidal channel

Table 1. List of experimental materials and dimensions of the landslide dams

No.	Weight ratio		Water content	θ_D	Discharge rate Q_{IN}
	Sand	Bentonite			
1	97.5%	2.5%	15%	50°	200 cm^3/s
2	97.5%	2.5%	10%		
3	97.5%	2.5%	5%		
4	100%	0%	15%		
5	97.5%	2.5%	10%	35°	

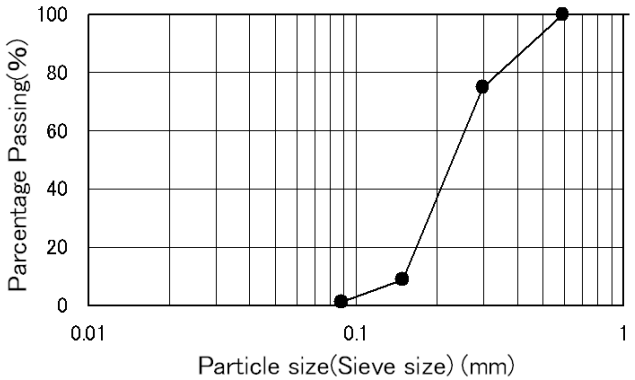

Fig. 2. Particle size distribution of the mixed sand used in the experiment

dams. Because landslides may not occur during landslide dam overflow, the likelihood of large, unexpected floods caused by landslide dam outbursts may also be low.

Figure 4 shows the temporal variations in sediment concentration; concentration were highest at the start of overtopping. The sediment concentration pattern resembled that of debris flow. The broken line represents the equilibrium sediment concentration of 23 % estimated by Takahashi (1980) using the formula:

$$C_d = \frac{\rho \tan\theta}{(\sigma - \rho)(\tan\phi - \tan\theta)} \tag{1}$$

where, C_d; sediment concentration of the debris flow, σ;density of sediment, 2.65 g/cm^3, ρ ;density of water, 1.0 g/m^3, θ ;gradient of the flume (11.3°), Φ; internal friction angle of the sediment (36°).

The outburst discharge was almost the same as that calculated by the experimental equation proposed

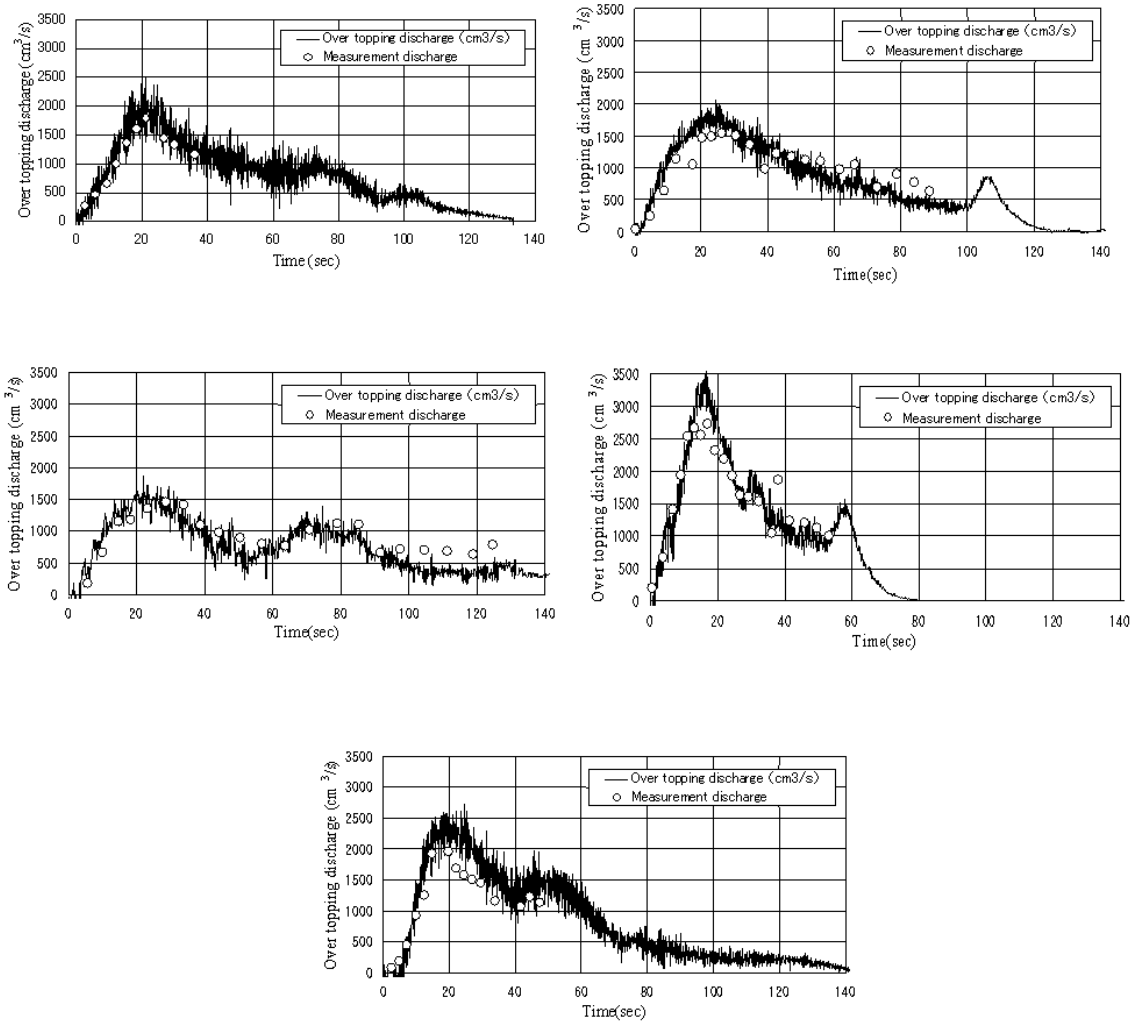

Fig. 3. The temporal variation of the overtopping discharge rate.

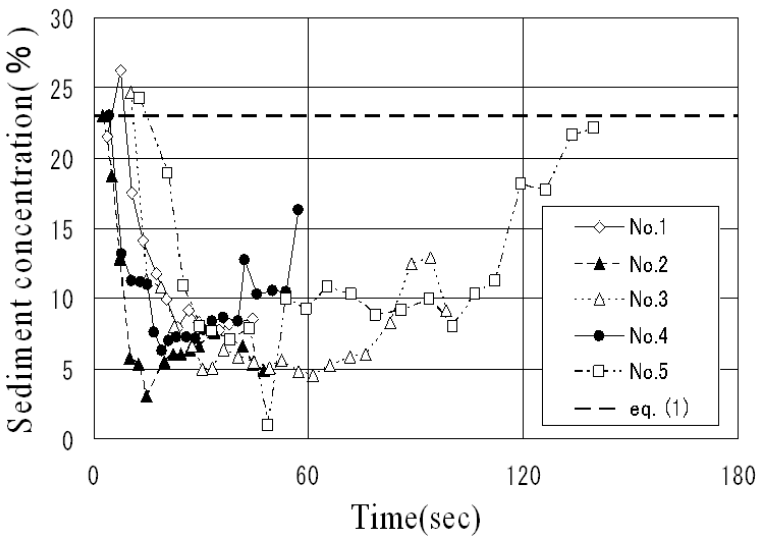

Fig. 4. The temporal variation in sediment concentration.

Table 2. Comparison between the measured maximum peak discharge rate and the calculated maximum peak discharge rate

No.	Measured maximum peak discharge rate at the end of channel when using both sand and water (cm^3/s)	Calculated maximum peak discharge rate by Eq.(2) (cm^3/s)
1	1772.5	1137～2275
2	1958.3	
3	1546.9	
4	2735.0	
5	1451.9	

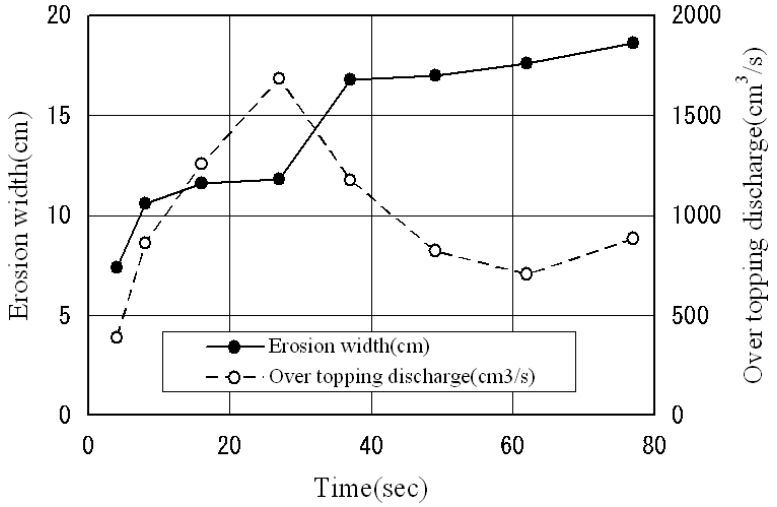

Fig. 5. Temporal variation in the erosion width and the overtopping discharge rate.

by Tabata et al. (2001, Table 2)

$$\frac{q}{q_{in}} = 0.542 \left\{ \frac{(gh^3)^{0.5}}{\tan\theta \cdot q_{in}} \right\}^{0.565} \tag{2}$$

where, q; oufflow discharge, q_{in} ; inflow discharge, g ; gravitational acceleration, h ; height of the landslide dam.

Figure 5 shows the temporal variation of erosion width and outflow discharge for Run No.5. The peak discharge appeared when the erosion width was rather constant. More detailed consideration of this phenomenon is necessary.

Analyzing the slope stability of landslide dams

As mentioned above, abrupt landslides may be rare during landslide dam outbursts. However, if, landslides occur when landslide dams are overflowing, resulting floods could be catastrophic. In this section, the stability of the downstream slopes of landslide dams was analyzed according to a soil mechanical method (Rotational slip method):

$$Fs = \frac{\sum\{c_i \cdot l_i + (W_i - u_i \cdot b_i)\cos\theta_i \cdot \tan\phi_i\}}{\sum W_i \cdot \sin\theta_i} \tag{3}$$

Table 3. List of calculation conditions of the landslide dam parameters

Landslide dam parameters	Preconditions
Height of landslide dam(m)	4, 8, 15, 30, 60, 120
Gradient of landslide dam's down stream slope (°)	30, 35, 45, 60, 75
Cohesion of landslide dam's material(kN/m^2)	10, 30, 40, 50
Internal friction angle(°)	10, 20, 30
Torrent gradient	1/65
Unit weight of landslide dam's material(kN/m^2)	18.0
Length of landslide dam(m)	1, 2, 5, 10, 20, 40, 80

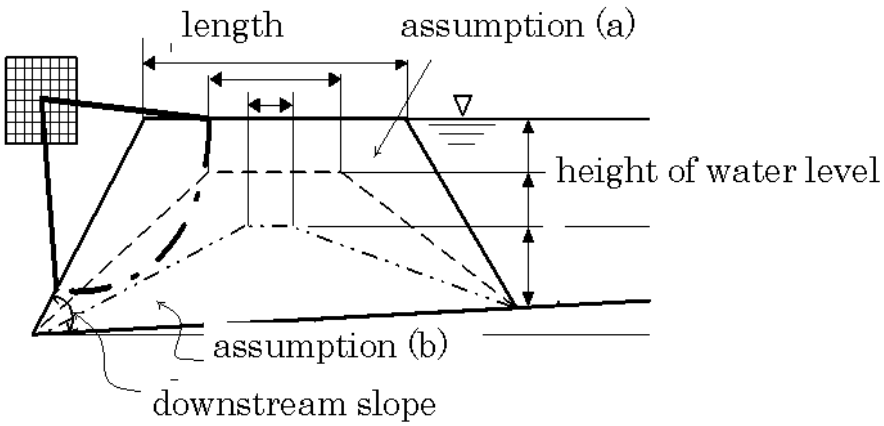

Fig. 6. Calculation model and parameters.

where, Fs ; safety factor of a slope, c_i ; cohesion of a slice i of a slip surface, li ; length of a slice i, W_i ; weight of a slice i, ui ; pore water pressure for a slice i, bi; width of slice i, θ; inclination of a slip surface from horizon, Φi; internal friction angle of a slice i.

The parameters for the calculation are downstream slopes, the soil mechanical parameters of the landslide dam materials, the longitudinal length of the landslide dam crest, and the landslide dam height. The calculation conditions of the parameters are given in Table 3.

Figure 6 illustrates a calculation model. We assumed the following things:

a) Landslide dams are filled with water and the dam bodies are saturated. The water levels are 3/4, 1/2 and 1/4 the dam height.

b) The dam material is homogeneous. The general values of the internal friction angle and cohesiveness are adapted.

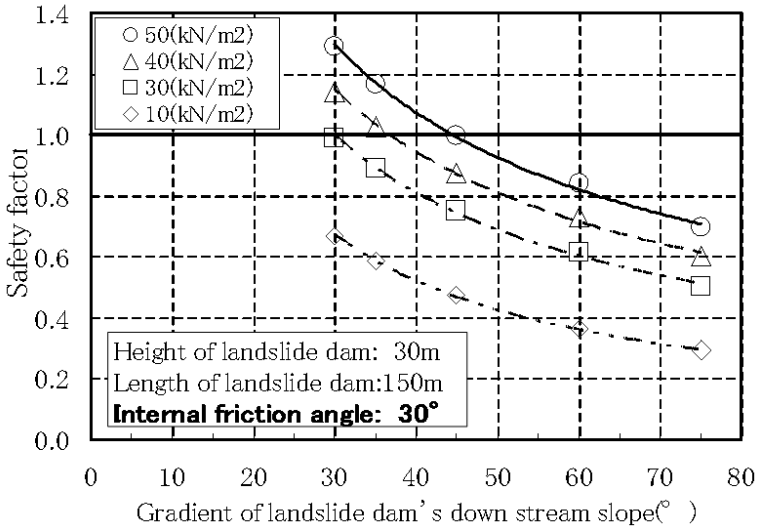

Fig. 7. Relationship between the downstream slope gradient of a landslide dam and the safety factor.

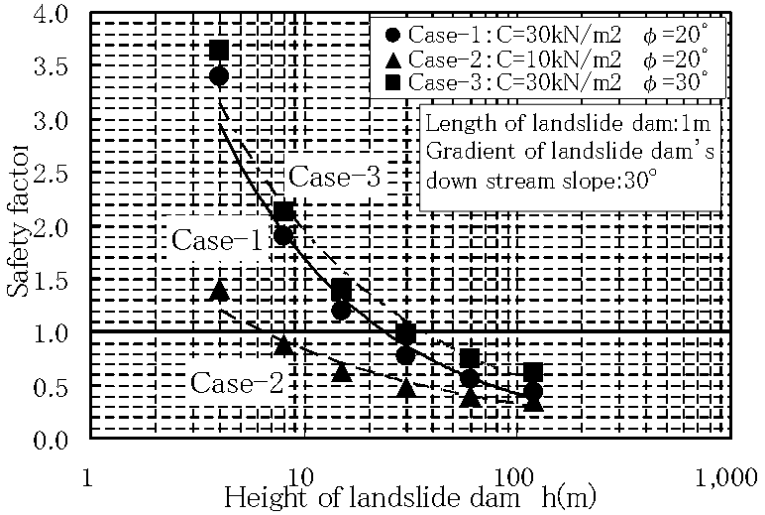

Fig. 8. Relationship between height of landslide dam and safety factor.

Influence of dam shapes and materials on slope stability

Figure 7 shows how the slope stability changed with the downstream slope gradient and cohesiveness under the following conditions: the dam height = 30 m, the dam length = 150 m and the internal friction angle = 30 degrees. Steeper downstream slopes made the dam body more unstable.

Influence of dam height on the slope stability

Calculations were carried out under the condition that a dam was filled with water. Figure 8 shows the results. A higher dam was the more unstable.

Influence of the dam water level on stability

Figure 9 shows that the longer longitudinal length of a landslide dam is more stable if the water level of the dam reaches the dam height. After a landslide has formed, it may be difficult to obtain the characteristics of the associated dam body or ascertain the strength of the dam material. However, the dimensions of a landslide dam can be easily and accurately obtained using laser profilers. The engineer can assume the soil properties based on experience and estimate the soil stability.

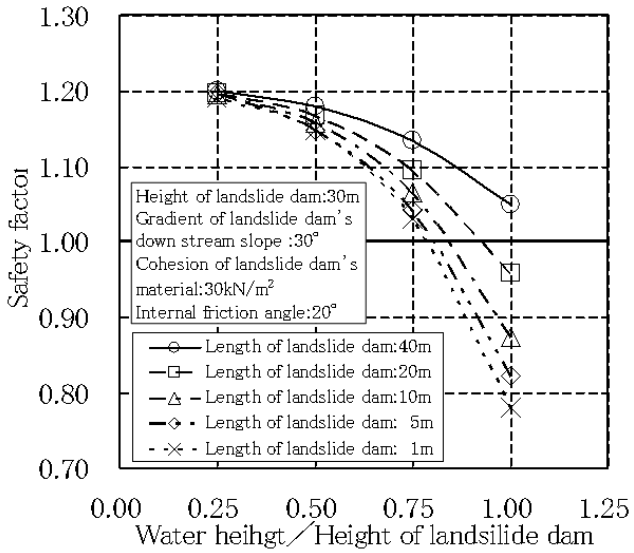

Fig. 9. Relationship among the seepage line poison, the landslide dam length, and the safety factor.

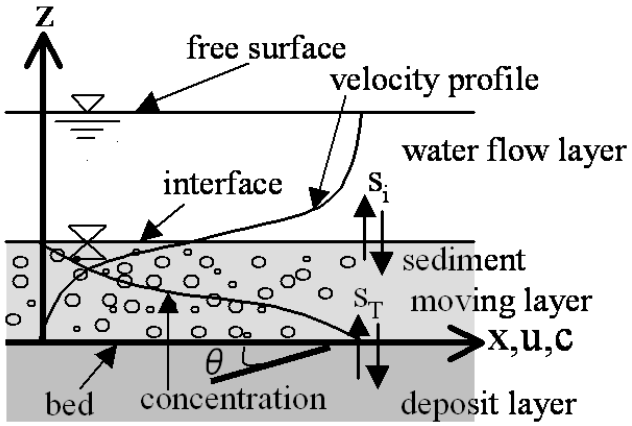

Fig. 10. A schematic diagram of the two the two-layer sediment transport.

Calculation of outflow discharge during outburst

Empirically and experimentally based methods can be used to predict the outflow discharge during landslide dam outbursts. A few mathematical models produce outflow hydrographs and can simulate outflow processes and predict discharge. This method has been applied to a real case that occurred in 1892 and has been relatively well studied.

The calculation model

We adapted the two-layer model developed by Takahama et al. (2000, 2002, 2004) which is applicable for immature debris flow to debris flow. Figure 10 illustrates the model. Volumetric values of the water layer per units of time and area through the interface are defined as SI. The governing equations are described below, where the suffixes w, s are represent the water layer and the moving sediment layer, respectively.

Continuous equations

(1) Entire moving layer

$$\frac{1}{B}\frac{\partial Bh}{\partial t}+\frac{1}{B}\frac{\partial B\nu h}{\partial x}=s_T \tag{4}$$

(2) Sediment layer

$$\frac{1}{B}\frac{\partial cBh}{\partial t}+\frac{1}{B}\frac{\partial cB\nu h}{\partial x}=c_* s_T \tag{5}$$

(3) Temporal change of torrent bed elevation

$$\frac{\partial z_b}{\partial t}=s_T \tag{6}$$

(4) Erosion rate

$$s_T=\nu\tan(\theta-\theta_e) \tag{7}$$

Equations of motion

(1) Water layer

$$\begin{aligned}&\frac{1}{B}\frac{\partial(\rho_w\nu_w Bh_w)}{\partial t}+\frac{1}{B}\frac{\partial(\rho_w\beta_w\nu_w^2 Bh_w)}{\partial x}-\rho_w s_I u_I\\ =\quad&\rho_w g h_w\sin\theta-\frac{\partial P_w}{\partial_x}-P_I\frac{\partial h_s}{\partial_x}-\tau_w\end{aligned} \tag{8}$$

(2) Moving sediment layer

$$\begin{aligned}&\frac{1}{B}\frac{\partial(\gamma'\rho_s\nu_s Bh_s)}{\partial t}+\frac{1}{B}\frac{\partial(\rho_s\beta_s\nu_s^2 Bh_s)}{\partial x}+\rho_w s_I u_I\\ =\quad&\rho_s g h_s\sin\theta-\frac{\partial P_s}{\partial_x}-P_I\frac{\partial h_s}{\partial_x}-\tau_w-\tau_b\end{aligned} \tag{9}$$

where ρ; averaged density, θ; torrent gradient, B; width, h; thickness of the moving layer, ν; mean velocity, g; gravitational acceleration, c; averaged sediment concentration, u_I; x-direction velocity at the interface P_w; pressure acting the water layer integrated from the interface to the free surface, P_s; pressure acting the sediment layer integrated from torrent bed to the interface, P_I; pressure at the $interface$, τ_w; shear stress to the interface, τ_b; shear stress to the torrent bed, s_T; erosion rate. Parameters, $\gamma, \gamma', \beta_s, \beta_w$ are correction factors for the vertical distributions of velocity, sediment concentration and density respectively and are all assumed to be unity here. The shear stress of the torrent bed and erosion rate were evaluated using the model found in Egashira et al. (1997).

Shear stress to the torrent bed

$$\tau_b = \tau_y+\rho_w f_s\nu_s|\nu_s| \tag{10}$$

$$\tau_y = \left(\frac{c_s}{c_*}\right)^{1/5}(\sigma-\rho_w)c_s g h_s\cos\theta\tan\phi_s \tag{11}$$

$$\tan\theta_{eq} = \frac{(\sigma-\rho_w)c_t}{(\sigma-\rho_w)c_t+\rho}\tan\phi_s \tag{12}$$

$$\begin{aligned}G_{yk} &= \frac{\tau_{ext(z=z_b)}-\tau_{yk(z=z_b)}}{\rho_w g h_s}\\ &= \{(\sigma/\rho_w-1)c_s+1\}\sin\theta_e-(\sigma/\rho_w-1)c_s\cos\theta_{eq}\left(\frac{c_x}{c_*}\right)^{1/5}\tan\phi_s\end{aligned} \tag{13}$$

$$\begin{aligned}W &= -Gy_s\\ &= \{(\sigma/\rho_w-1)c_s+1\}\sin\theta_{eq}-(\sigma/\rho_w-1)c_s\cos\theta_{eq}\tan\phi_s\end{aligned} \tag{14}$$

$$f(c_s) = k_f\frac{(1-c_s)^{5/3}}{c_s^{2/3}}+k_g\frac{\sigma}{\rho_w}(1-e^2)c_s^{1/3} \tag{15}$$

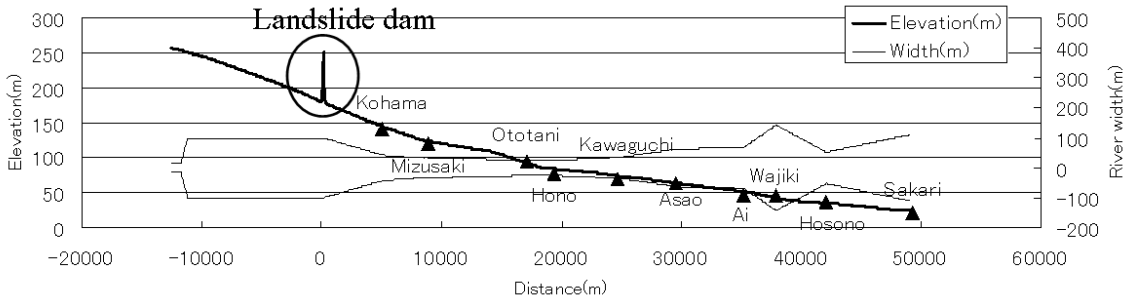

Fig. 11. Longitudinal profile and with of the Naka-gawa river.

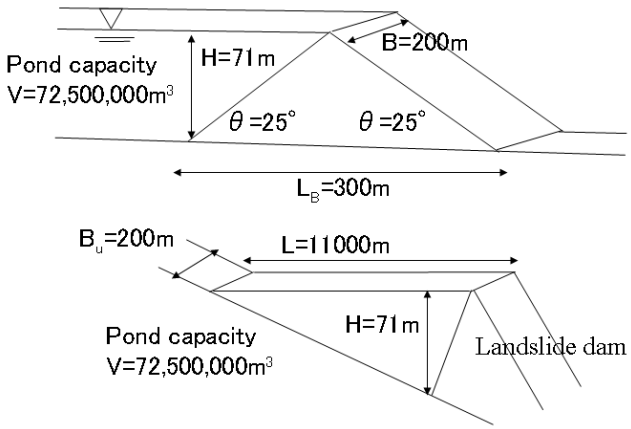

Fig. 12. Dimensions of Taka-iso-yama landslide dam.

$$\text{when } G_{yk} \neq 0$$

$$f_s = \frac{225}{16} f(c_s) G_{yk}^4 (W + G_{yk}) \left\{ W^{5/2} - (W + G_{yk})^{3/2} \left(W - \frac{3}{2} G_{yk} \right) \right\}^{-2} \left(\frac{h_x}{d} \right)^{-2} \tag{16}$$

$$\text{when } G_{yk} = 0$$

$$f_s = 4 f(c_s) \left(\frac{h_s}{d} \right)^{-2} \tag{17}$$

where σ; sediment density, θ_{eq}; equilibrium gradient corresponding to the average density of the entire layer, ϕ_s; internal friction angle of the sediment (35.0°), $k_f = 0.25, k_g = 0.0828$, e; repulsion factor, d; mean diameter.

Bed gradient of the Naka-gawa river that we picked out as an example for the case study is flat and resistance law for bedload transport is needed. We used Manning's resistance law when sediment concentration becomes less than 0.02 as Takahashi and Kuang did (Takahashi and Kuang, 1988).

$$\tau_b = \frac{\rho g n^2 \nu |\nu|}{h^{1/3}} \tag{18}$$

where n is Manning's roughness coefficient.

Calculation Conditions

(1) River channel

The calculations encompassed the area extending from 12,500 m upstream to 50,000 m downstream from the landslide dam as shown in Fig. 11. The river bed was assumed to be rigid, except for the landslide dam. The cross sections were assumed to be rectangular in shape. The river elevations and widths were determined based on Inoue et al. (2005), and no erosion was assumed for the river banks.

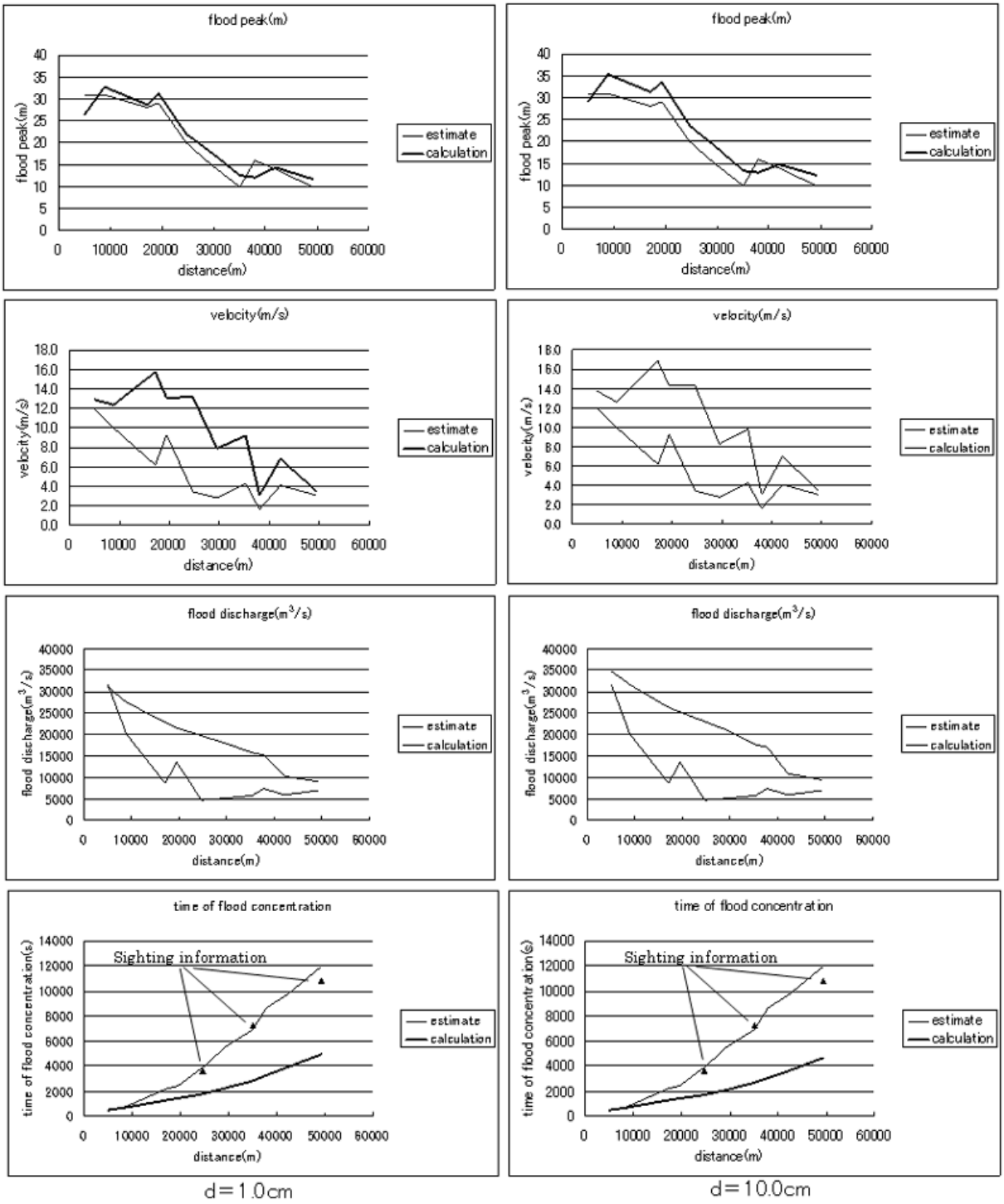

Fig. 13. Comparisons of calculated results and data reported from the field survey.

(2) Inflow rate

Inoue et al. (2005) estimated the inflow rate to the landslide dam based on the pond capacity and filling time. We adopted his value, 388m^3/s (= pond capacity; 72.50 million m^3 / filling time; 1.87 × 105 s), and applied this value constantly at the upstream end of the calculation reach.

(3) Others

The landslide dam was 71 m high and had a pond volume of 72.50 million m^3. The width of the landslide dam (B) and its base length (LB) are shown in Figure 12 based research by Inoue et al. (2005). The width of the pond was 200 m (= pond capacity; 72.50 million m^3 /{(distance; 11,000 m × height; 71 m) /

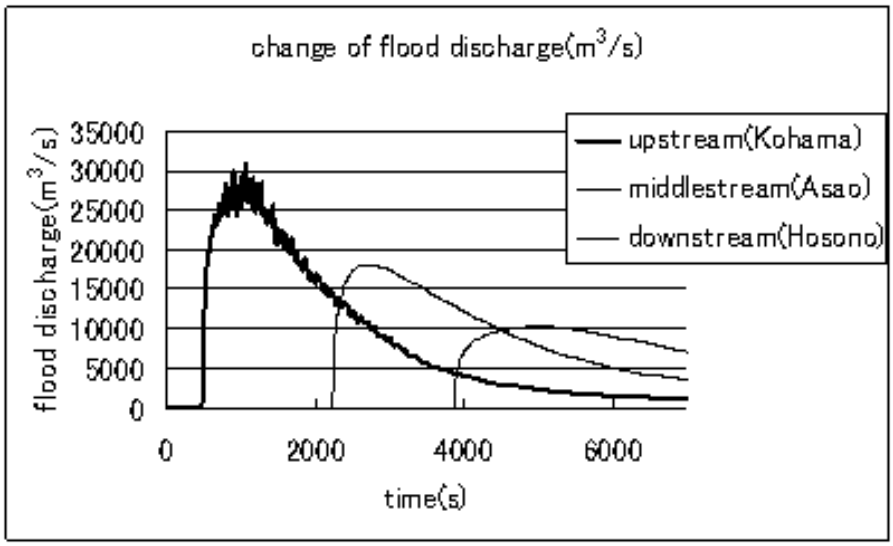

Fig. 14. Changes of flood discharge at three sections.

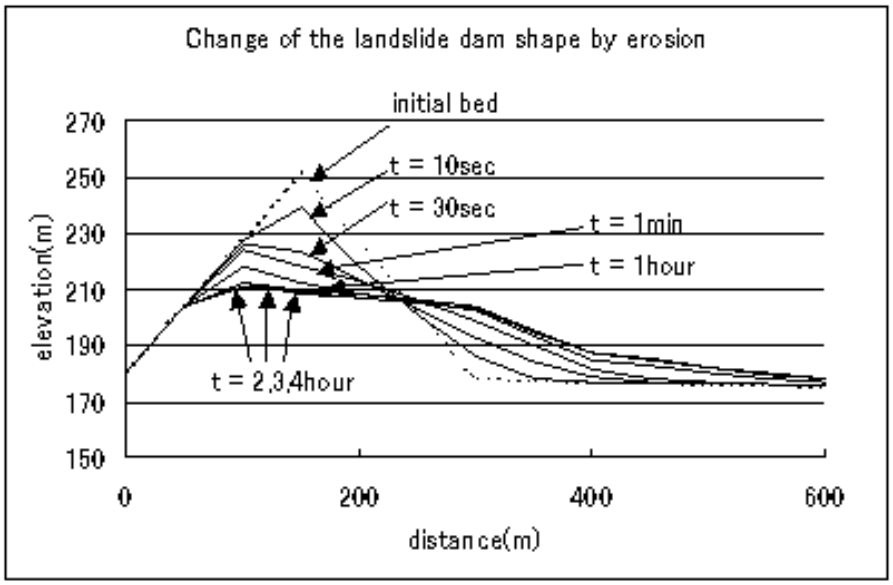

Fig. 15. Change of the landslide dam shape by erosion.

2}), and two mean diameters were assumed for the sediment 1 cm and 10 cm. The internal friction angle was assumed to be 35° and Manning's roughness coefficient was 0.05.

Calculated results

Figure 13 shows the calculated results compared with the estimation of Inoue et al. (2005). Applying sediment diameters of 1 and 10 cm did not result in large differences. The flood water level was well calculated, with the results slightly higher than levels estimated just below the landslide dam. The calculated flow velocity was higher than the estimated values. Observations were reported by by Terado (1970). The reason for the faster velocity is unclear. One possibility is that the actual river is sinuous, while the calculation was based on a straight channel.

Peak flow discharges at three sections (upstream, midstream and downstream) are shown in Fig. 14. The peak discharge decreased with distance downstream. Figure 15 shows erosion of the landslide dam, while Fig. 16 illustrates temporal water level changes. Considerable erosion of the dam occurred early, but the dam shape did not change much at later times.

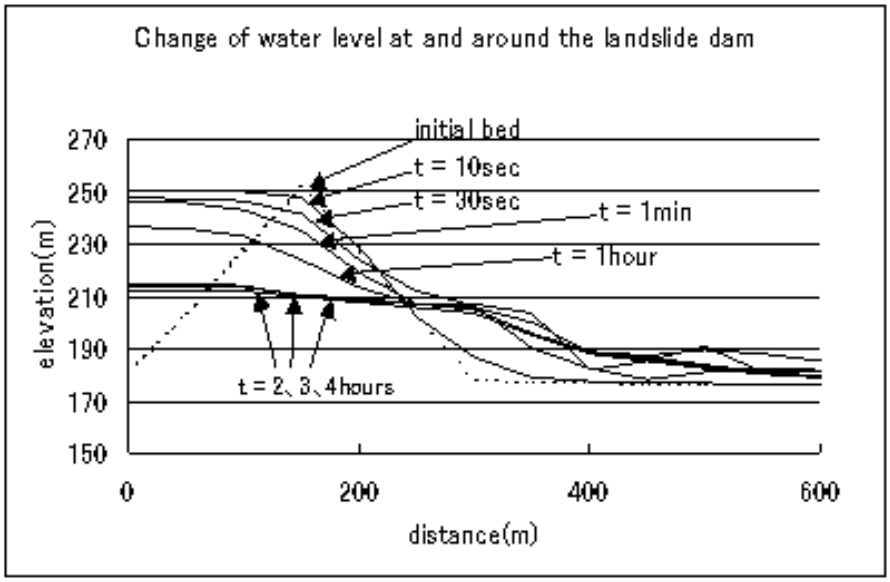

Fig. 16. Change of water level at and around the landslide dam.

Conclusions

Erosion processes associated with landslide dam outburst were investigated using flume experiments. Mechanisms forming flood peaks were made clear. Numerical analyses of slope stability for various landslide dam dimensions and conditions were also conducted. What kind of landslide dams are more unstable was known through the analyses. A numerical simulation model was developed to estimate both peak flow discharge and the flow hydrograph. The method was applied to a historical flood resulting from the outburst of the Taka-iso-yama landslide dam in the Naka-gawa River of Tokushima, Japan. The calculated results agreed well with the field survey data. This modeling method will be applied to actual risk management activities. Topographic information on new landslide dams obtained using a laser profiling technique will be input to the model calculations.

The authors thank the Sabo Technical Center for their support of this research. We also thank Dr. Akira Oda and Mr. Yuji Hasegawa of the Construction Research Laboratory for their assistance with the flume experiments, as well as Mr. Tatsuhei Ito of the Sabo Frontier Foundation, Dr. Jun-ichiro Takahama of Gifu University, and Mr. Kousuke Yoshino of Asia Air Survey Co. Ltd. for their kind assistance with the slope stability analysis and computer simulations.

References

Egashira, S., Miyamoto, K. and Ito, T. (1997) *Bed-load rate in view of two phase flow dynamics*, Annual Journal of Hydraulic Engineering, JSCE, Vol.41, p.789–794. (In Japanese with English abstract)

Inoue, K., Mori, T., Itou, T. and Kabeyama, Y. (2005) *Outbursts and disasters of Takaisoyama and Hose landslide dams (1892) in East Shikoku*, Journal of the Japan Society of Erosion Control Engineering, 58–4, p.2–12. (In Japanese with English abstract)

Tabata, S., Ikeshima, T., Inoue, K. and Mizuyama, T. (2001) *Study on prediction of peak discharge in floods caused by landslide dam failures*, Journal of the Japan Society of Erosion Control Engineering, 54–4, p.73–76. (In Japanese with English abstract)

Takahama, J., Fujita, Y. and Kondo, Y. (2000) *Analysis method of transitional flow from debris flow to sediment sheet flow*, Annual Journal of Hydraulic Engineering, JSCE, Vol.44, p.683–686. (In Japanese with English abstract)

Takahama, J., Fujita, Y., Kondo, Y. and Hachiya, K. (2002) *Two layer model for analysis of deposition and erosion processes of debris flows*, Annual Journal of Hydraulic Engineering, JSCE, Vol.46, p.677–682. (In Japanese with with English abstract)

Takahama, J., Fujita, Y. and Yoshino, K. (2004) *Debris flow considering vertical distribution of velocity and concentration*, Annual Journal of Hydraulic Engineering, JSCE, Vol.48, p.677–682. (In Japanese with with English abstract)

Takahashi, T. (1980) *Debris flow on prasmatic open channel*, Journal of Hydraulic Engineering, ASCE, 106, No. HY3, p.381–396.

Takahashi, T. and Kuang, S.F. (1988) *Hydrograph prediction of debris flow due to failure of landslide dam*, Annuals, Disas. Prev. Res. Inst., Kyoto Univ., No.31 B-2, p.601–615. (In Japanese with with English abstract)

Terado, T. (1970) *Takaisoyama landslide in Tokushima and dam break disaster prevention*, Geographical Sciences, 14, p.22–28. (In Japanese)